Optically defined plasmonic waveguides in crystalline semiconductors at optical frequencies

Herman M. K. Wong* and Amr S. Helmy

The Edward S. Rogers Sr. Department of Electrical and Computer Engineering, University of Toronto, 10 King's College Road, Toronto, Ontario M5S 3G4, Canada
**Corresponding author: herman.wong@mail.utoronto.ca*

Received December 5, 2012; revised February 11, 2013; accepted February 18, 2013; posted February 22, 2013 (Doc. ID 180926); published March 25, 2013

High intensity optical excitation to transform a crystalline semiconductor into a plasmonic metal at near-infrared wavelengths is theoretically investigated. A calculated intensity of 51.46 GW/cm^2 is sufficient to transform GaAs into metal at 1.55 μm to support plasmonic modes. A practical nanoscale plasmonic gap waveguide is designed based on the GaAs/GaN materials system, demonstrating the capability of obtaining plasmonic waveguiding by high intensity optical excitation. The propagation characteristics of the plasmonic gap mode in the designed waveguide can be dynamically tuned over a broad range of values by varying the intensity of the pump excitation using modest average powers between 15 and 75 mW.

OCIS codes: 250.5403, 250.4390.

1. INTRODUCTION

Over the past decade, there has been renewed interest in the subject of surface plasmons with a marked increase in the research activities in the field. This has been driven by the advancement of nanofabrication technologies, the availability of highly sensitive nanoscale optical characterization techniques, and the increase in computational capacity that allows one to numerically investigate complex plasmonic structures. These capabilities have enabled the development of various exciting applications in areas, such as subwavelength waveguiding, enhancement of emission processes, optical nonlinearities, spectroscopy, sensing, metamaterials, and imaging [1].

A serious limitation of plasmonics is that the propagation of modes in the vicinity of metal surfaces suffers from high ohmic loss as a result of the damping of collective electron oscillations, leading to propagation lengths on the order of only tens to hundreds of microns. In addition to this intrinsic ohmic loss due to free carriers in the metal, conventional techniques such as evaporation or sputtering that are used to create polycrystalline metal films tend to create films with high surface roughness and grain boundaries [2], which cause scattering loss for surface plasmon polaritons (SPPs). One promising technique to significantly reduce the surface roughness would be the epitaxial growth of semiconductor-metal heterostructures, such as in [3] where molecular beam epitaxy (MBE) is used to fabricate AlAs–NiAl–AlAs heterostructures. Intermetallics such as NiAl can be utilized as an alternative material for plasmonics, but many materials in this class exhibit poor plasmonic performance due to the low frequency of their interband transitions [4]. The growth of monocrystalline gold thin films with 0.2 nm root-mean-square roughness, which is an order of magnitude lower than with traditional sputtering techniques, has also been demonstrated based on epitaxial deposition [5]. However, these approaches require a substrate with crystalline lattice that is matched with the lattice constant of the deposited metal; for gold deposition, the ionic crystal lithium fluoride is used, and these substrate materials are in general not compatible with traditional semiconductor fabrication processes. Another method to compensate for metal loss is by replacing the passive dielectric with an active gain medium. For example, gain assisted SPP propagation in dielectric-loaded SPP waveguides has been demonstrated recently [6]. Reducing losses using a hybrid plasmonic waveguide is also predicted [7], where propagation lengths higher than that of conventional plasmonic modes are achievable while maintaining subwavelength confinement in the spacer region. However, the fundamental limitation in these alternative plasmonic structures is still the surface roughness of the metal layers.

The use of an all-semiconductor structure for plasmonic waveguides can alleviate losses caused by the high surface roughness of metallic layers and the material defects in dielectric layers grown on top of the metal surface. This is because single crystal semiconductors are readily available and they have atomically smooth interfaces. Semiconductors can also be very precisely structured down to the nanometer length scale in both vertical and horizontal directions, using a combination of techniques such as MBE for material growth and electron beam lithography for patterning. Using semiconductors that are compatible with traditional fabrication processes can thus pave the way for the integration of plasmonic devices with well-established electronic devices, and also with more conventional photonic devices, which have already been successfully implemented in semiconductor material systems such as silicon [8].

One important characteristic of semiconductors is that their carrier concentrations can be tuned over a wide range by different methods, such as doping, electrical injection, and optical excitation. This is not possible in metals as all the valence electrons that contribute to the permittivity are delocalized as described by the Drude model. As such there

are no additional bound electrons that can be promoted to the conduction band and contribute to increasing the free carrier concentration. The Drude model that describes the permittivity of a material containing free carriers is given in Eqs. (1) and (2) below.

$$\varepsilon(\omega) = \varepsilon_\infty\left(1 - \frac{\omega_p^2}{\omega^2 + i\gamma\omega}\right), \tag{1}$$

$$\omega_p^2 = \frac{ne^2}{\varepsilon_o m_e}. \tag{2}$$

The Drude model gives the dielectric permittivity as a function of the angular frequency ω of the electromagnetic (EM) wave excitation, where ε_∞ is the high frequency dielectric constant, γ is the phonon damping constant, and ω_p is the plasma frequency given by Eq. (2). The plasma frequency is a function of the free carrier concentration n and the carrier effective mass m_e, which is specific to the material. At a fixed frequency, increasing the free carrier concentration would decrease the real part of the permittivity and increase the imaginary part. Therefore, it is possible to turn a semiconductor into a metal by increasing the free carrier concentration past the point when the real part of the permittivity becomes negative, which is a requirement for a material to be optically metallic and hence plasmonic [1]. The tunability of the carrier concentration and thus plasmonic properties in a semiconductor that has been rendered metallic is another notable advantage over metals.

This work presents a feasible design approach to demonstrate all-semiconductor structures as a viable plasmonic material platform in the near-infrared (NIR) and visible frequencies using optical excitation. Section 2 discusses demonstrations of plasmonic waveguides in all-semiconductor structures for operating frequencies ranging from the terahertz (THz) to visible regions. Section 3 presents an analysis of optical excitation to induce plasmonic behavior in mainstay semiconductors such as GaAs and clearly shows that it is feasible with existing technologies. Section 4 discusses the possibility of using optical excitation to define a practical plasmonic gap waveguide and dynamically tune its properties [9]. Finally, the wider implications for functional plasmonic devices will be discussed.

2. PLASMONICS IN SEMICONDUCTORS

Plasmonic modes have been observed at THz frequencies in semiconductors for applications in sensing [10], waveguiding [11], and transmission through subwavelength apertures [12]. At THz frequencies, metals have very large complex permittivities, which enable the realization of plasmonic waveguides. Semiconductors, on the other hand, have much lower free carrier concentrations, and thus the magnitude of the real part of the permittivity is much lower. As a result, SPPs are more tightly bound at semiconductor–dielectric interfaces at THz frequencies [11], which is advantageous for many applications. For small bandgap semiconductors such as InSb, the smaller values of the real part of the permittivity and the plasma frequency means that plasmonic modes are confined to a distance from the semiconductor surface of roughly 2 orders of magnitude smaller, at $\sim 2.4 \times 10^{-4}$ m compared to the confinement distance for gold that is $\sim 2.5 \times 10^{-2}$ m. However, the stronger plasmonic mode confinement for InSb leads to a shorter propagation length at ~1.5 μm, which is more than 3 orders of magnitude less than in gold.

The challenge in sustaining SPPs at higher frequencies is that it is difficult to induce very high carrier concentrations in semiconductors; in the NIR and visible frequencies, the required carrier density is on the order of 10^{21} cm^{-3}; for conventional semiconductors such as Si, Ge, and AlGaAs, the lower solubility limit of dopants means that it is difficult to dope beyond 10^{20} cm^{-3}. One promising class of materials for plasmonics at NIR frequencies is doped oxide semiconductors such as zinc oxide and indium oxide, as heavy doping to the 10^{21} cm^{-3} level is possible due to their high solid solubilities of dopants. Negative refraction in the NIR has been reported previously using a superlattice made out of alternating subwavelength layers of AZO/ZnO [13]. Another material that exhibits even higher carrier concentrations than doped oxide semiconductors would be titanium nitride, which means that it is suitable to serve as a material for plasmonic waveguides even in the visible region [14]. One drawback of oxide semiconductors is that their properties are strongly dependent on the fabrication procedures [15], such as the requirement of precise control of temperature and oxygen partial pressure, as well as doping during pulsed-laser deposition of thin films. Moreover, there are still outstanding issues regarding the compatibility of this class of materials with more traditional semiconductors such as Si and AlGaAs. In another study, it was theoretically shown that InAs heterostructures can be utilized for plasmonics in the mid-infrared frequencies range [16]. Electrical injection was used to increase the free carrier density and thus induce metallic behavior.

A pressing question that begs answering is whether mainstay semiconductors such as Si and AlGaAs can be induced to become metallic and thus be used as plasmonic materials at NIR and visible frequencies. Achieving this task through doping is not likely given the solubility limit of dopants in conventional semiconductors.

3. OPTICAL EXCITATION TO ACHIEVE PLASMONIC WAVEGUIDES AT NIR AND VISIBLE FREQUENCIES

Optical excitation is another route to increase the free carrier concentration in a semiconductor, and thus it is a promising alternative for transforming a conventional semiconductor into a material fit for plasmonic waveguides. One advantage of using optical excitation is that it would enable plasmonic waveguides to be defined dynamically at arbitrary locations on a sample. By launching pump light through a patterned photomask from the top, only the illuminated tracks on the sample would become the plasmonic waveguide circuitry. It is also possible to tune the properties of the plasmonic mode during device operation, as will be shown subsequently in this paper.

Plasmonic behavior of dielectric thin films at optical frequencies has been theoretically shown in previous work, by the use of high electric fields that can be achieved with femtosecond (fs) pulses [17]. The effect has also been shown experimentally, such that silica becomes a conductor using ultrahigh intensity few-cycle optical pulses [18,19]. The metallization effect is caused by strong, adiabatically varying

electric fields on the order of 0.1 V/Å, which corresponds to wave intensities of $I \sim 0.1 - 1$ TW/cm^2. In a thin dielectric film of a few to tens of nanometers thick, the electron energy states are quantized, with the valence band states occupied, and the conduction band states empty. As the electric field is increased, two fundamental phenomena occur. First, the conduction and valence band edges become tilted across the thin film thickness, such that conduction band (electron) states will be pushed toward one film surface and valence band (hole) states are moved toward the opposite surface [20]. Simultaneously, the conduction-valence bandgap decreases due to the linear Stark effect [17] and completely closes at the field needed for metallization on the order of 0.1 V/Å. Prior to reaching the field required for metallization, the bandgap already becomes quite small, but the spatial separation of the conduction and valence band states due to the high electric field means that transitions between these two bands are highly suppressed. However, as the electric field is increased adiabatically past the metallization field, an anticrossing between the bottom conduction band and top valence band edges occurs [21], resulting in conduction band states originally at one surface of the thin film to exist at the opposite surface, where they spatially overlap with the valence band states. This allows for electron transitions at low frequencies, corresponding to the material resonance shifting to the NIR and visible regions of the spectrum, which means that the real part of the permittivity is negative at NIR and visible frequencies, a characteristic of optically metallic materials.

In the previously described method of metallization, plasmonic behavior is exhibited only in a narrow spectral range near the shifted material resonance of the dielectric thin film, which is in the NIR or visible region due to the high electric field of an ultrashort optical pulse. This is fundamentally different from a Drude metal, in which plasmonic behavior would be present for all wave frequencies lower than the plasma frequency of the free carriers in the metal. As will be shown next, the optical intensities to achieve sufficient carrier densities in semiconductors for plasmonic behavior is on the same order of magnitude as that required by the method of high electric fields in dielectric thin films, which would be around hundreds of GW/cm^2. However, the technique based on high electric fields requires a thin film of nanometers thickness to be used, and the ultrashort pulse must have a temporal duration determined by the film thickness [17]. On the other hand, the technique described in this work is based on high optical intensity excitation to generate free carriers in semiconductors, thus it is not limited by these factors even though ultrashort pulses are still necessary to achieve the required intensities.

It is essential initially to determine the necessary conditions for optical excitation to induce a sufficiently high carrier concentration in a semiconductor to give rise to the plasmonic effect, namely, the optical intensity required for a given semiconductor material. High-intensity picosecond pulsed lasers can produce electron-hole plasmas that is essentially free carriers with concentrations on the order of 10^{20} cm^{-3} in undoped semiconductors such as GaAs [22]. There has also been work on laser excited electron-hole plasmas up to the 10^{21} cm^{-3} concentration range in semiconductors such as silicon, both theoretically [23] and experimentally [24]. It is also possible to reach carrier densities in semiconductors of above 10^{22} cm^{-3} with fs laser pulses [25].

To calculate the required excitation intensity to reach a certain carrier concentration, we begin with the rate equation for the carrier concentration, as shown in Eq. (3). For the case of a single pump beam, the two forces driving the change in carrier concentration are the pump rate P and the recombination rate R.

$$\frac{dn}{dt} = P - R = \frac{\alpha_0 I + \alpha_2 I^2}{h\nu} - (An + Bn^2 + Cn^3). \tag{3}$$

Considering the case of steady state, there is no net generation of carriers so $dn/dt = 0$, and the pump rate can be equated with the recombination rate. The pump rate is dependent on the excitation intensity I, and it is dominated by linear absorption α_0 at low intensities and two-photon absorption (TPA) α_2 at high intensities. It is also dependent on the frequency ν of the excitation radiation. The recombination rate is dependent on the carrier density and the coefficients A, B, and C, which denote nonradiative recombination, radiative recombination, and Auger recombination, respectively. These parameters are specific to the material under investigation.

As the excitation intensity is increased, the carrier concentration in the conduction band increases while the concentration of carriers in the ground state where they can absorb light is depleted. This leads to the saturation of linear absorption of the excitation pump. Similarly, there are a finite number of excited states in which carriers can be promoted by the TPA process, so TPA also saturates at sufficiently high excitation intensities. Mathematically, absorption saturation is represented by the intensity dependence of α_0 and α_2, such that they decrease as the intensity is increased. The intensity dependence of the linear absorption coefficient can be expressed as

$$\alpha_0(I) = \frac{\alpha_0'}{1 + I/I_{s0}}, \tag{4}$$

where α_0' is the linear absorption coefficient at low intensities ($\sim 1.33 \times 10^6$ m^{-1} for GaAs at $\lambda = 800$ nm) when saturation effects are negligible and I_{s0} is the linear absorption saturation intensity, which for a temporal Gaussian beam profile is given by

$$I_{s0} = \frac{\hbar\omega}{\tau\sigma_0'}\sqrt{\frac{12 \ln 2}{\pi}}. \tag{5}$$

In Eq. (5), τ is the lifetime of the upper state ($\sim 10^{-8}$ s for GaAs), or the duration of the excitation pulse if it is shorter than the upper state lifetime, ω is the excitation angular frequency, and $\sigma_0' = \alpha_0'/N_0$ is the unsaturated linear absorption cross section where N_0 is the number density of excitable species ($\sim 4.42 \times 10^{22}$ cm^{-3} for GaAs) [26]. The saturation of TPA in a bulk semiconductor can be modeled by the hyperbolic approximation [26]

$$\alpha_2(I) = \frac{\alpha_2'}{1 + I^2/I_{s2}^2}, \tag{6}$$

such that α_2' is the TPA coefficient at low intensities ($\sim 2 \times 10^{-9}$ m/W for GaAs at $\lambda = 800$ nm), and I_{s2} is the TPA saturation intensity given by

$$I_{s2} = \sqrt{\frac{2\hbar\omega}{\tau\sigma_2'}} \sqrt{\frac{12 \ln 2}{\pi}}, \tag{7}$$

where $\sigma_2' = \alpha_2'/N_0$ is the unsaturated TPA cross section. Equations (5) and (7) yield the linear absorption and TPA saturation intensities in GaAs of 6.71 TW/cm^2 and 945 GW/cm^2, respectively, at the pump wavelength of $\lambda = 800$ nm. Thus, the effective absorption coefficient $\alpha_{\text{eff}} = \alpha_0 + \alpha_2 I$ of GaAs, taking into account both linear absorption and TPA, peaks at an excitation pump intensity close to the TPA saturation intensity I_{s2}, which is approximately $\alpha_{\text{eff}} = 1.06 \times 10^5$ cm^{-1}.

The compound semiconductor GaAs is used as an example for the subsequent calculations. By solving the wave equation at the boundary between a metal and a dielectric, the dispersion relation for a single interface SPP can be derived [1], and it is given by

$$\beta = \frac{\omega}{c} \sqrt{\frac{\varepsilon_M \varepsilon_D}{\varepsilon_M + \varepsilon_D}}, \tag{8}$$

where ε_M and ε_D are the relative electric permittivities of the metal and dielectric, respectively. To propagate SPPs at the metal–dielectric interface, the propagation constant β must be a real value, which sets the condition that $\varepsilon_M + \varepsilon_D < 0$, or $|\varepsilon_M| > |\varepsilon_D|$ since ε_M is a negative value. If the GaAs/GaN materials system, which is suitable for designing an optically defined plasmonic waveguide as will be discussed in Section 4, is considered for demonstrating the plasmonic effect at high intensity optical excitation, then sustaining SPPs at a GaAs–GaN interface would require that the absolute value of ε_M for metallic GaAs is greater than ε_D for GaN. Since GaN has a maximum ε_D of ~9.7, ε_M for GaAs when rendered metallic is set at −12 in subsequent calculations. From Eqs. (1) and (2), the required carrier concentration for the relative permittivity of GaAs to reach a value of −12 at the telecommunications wavelength of 1550 nm is approximately 7.2×10^{20} cm^{-3}.

Practically, the intensity levels calculated above are achievable only in laser systems with ultrafast pulses, such as commercial Ti-sapphire lasers. As an example, a 150 fs pulsed laser with 500 mW average power and a repetition rate of 78 MHz produces a peak intensity on the order of several TW/cm^2, which is sufficient for inducing plasmonic behavior in GaAs at optical frequencies. It is also noted that high peak intensity ultrafast lasers in the fs regime can cause irreversible damage to semiconductor materials via a nonthermal lattice disordering process, which has a critical free carrier density of $n_{\text{cr}} \sim 10^{22}$ cm^{-3} [25,27]. This phenomenon has been shown in several experimental reports, where irreversible laser-induced phase transition in semiconductors is caused by fs pulses from commercial subpicosecond Ti:sapphire laser systems [28] or passively mode-locked dye lasers [29,30]. Thus, the peak intensity of the excitation beam must have an upper limit such that it induces a free carrier density less than n_{cr}. An ultrafast fs regime pulsed excitation is on a much shorter time scale than the recombination time (upper state lifetime) of the carriers, which is on the order of a few nanoseconds for direct bandgap semiconductors. On the fs time scale, steady state would not be reached, and thus the recombination effects are negligible. The carrier density n generated by an ultrafast pulse of a certain peak intensity can then be approximated by multiplying the pump rate P by the pulse duration t_p:

$$n = \frac{\alpha_0 I + \alpha_2 I^2}{h\nu} \times t_p. \tag{9}$$

For a 150 fs duration excitation pulse at $\lambda = 800$ nm, the required intensity to reach the carrier density of 7.2×10^{20} cm^{-3} for plasmonic behavior at 1.55 μm is approximately 51.46 GW/cm^2. This translates to an average optical power of only 3 mW if a 78 MHz repetition rate pulsed laser is used, considering the excitation spot diameter of 800 nm. As a comparison, at the pump intensity corresponding to the maximum effective absorption coefficient in GaAs, the carrier density achieved is $\sim 8 \times 10^{22}$ cm^{-3}, which is 2 orders of magnitude higher than that required for inducing plasmonic behavior. This means excitation intensities of well below the absorption saturation values in GaAs are sufficient to demonstrate the plasmonic effect. Under excitation by a high intensity pump pulse, the illuminated section of GaAs material becomes amenable to SPP excitation by a 1550 nm wavelength signal beam. The time duration where the SPP excitation lasts is on the order of the free carrier lifetime or, equivalently, the upper state lifetime. As shown above, it is quite feasible for conventional semiconductors to be used as materials supporting plasmonic modes from NIR to visible frequencies based on optical excitation, as the required optical intensities are readily achievable with commercially available ultrafast laser systems.

4. PUMP EXCITATION INTENSITY-DEPENDENT PLASMONIC MODE PROPERTIES

A. Semiconductor Plasmonic Waveguide Design

From the preceding analysis, high intensity optical excitation as a route to achieve plasmonic behavior in semiconductors at optical frequencies is found to be quite feasible. To demonstrate the proposed technique, a practical waveguide structure is designed such that a pump excitation mode causes certain regions of the cross section to become metallic, and a probe plasmonic mode can exist in the structure as a result. The main criteria for the waveguide design are that it should be amenable to actual fabrication with currently existing technologies and that the probe signal should only be detected at the output when the pump excitation is present in order to clearly identify the existence of a plasmonic mode. Ideally, the waveguide cross section would have submicron dimensions with the potential for further downscaling, because one of the main attractions of plasmonics technology is that optical devices can be reduced to subdiffraction-limited sizes.

A major challenge in the semiconductor plasmonic waveguide design is to find a materials system in which only the regions of the waveguide cross section intended to be rendered metallic become metallic as a result of pump excitation. For example, if the GaAs/AlGaAs material system is used to implement the waveguide, at the ultrahigh intensities required for plasmonic behavior in GaAs, the surrounding $Al_xGa_{1-x}As$ regions would exhibit such a high carrier concentration that

it too would become metallic, regardless of the fraction of aluminum content. While the fraction of aluminum of the surrounding $Al_xGa_{1-x}As$ can be chosen to avoid single-photon absorption at the pump wavelength, TPA would always exist because AlGaAs over the entire range of possible aluminum content has a bandgap energy that is less than twice that of GaAs. To avoid TPA in the surrounding regions, a material with a bandgap energy that is more than two times that of GaAs must be used. A promising candidate material would be gallium nitride (GaN), which has a direct bandgap energy of 3.4 eV, well over twice the bandgap energy of GaAs of 1.424 eV. Over the past few years, high quality and thickness GaN growth on a GaAs substrate using plasma-assisted MBE has been demonstrated with continual improvements in wafer size, crystalline quality, and growth rate [31], showing that the GaAs/GaN materials system is quite feasible for implementing the semiconductor plasmonic waveguide design in this work.

The semiconductor plasmonic waveguide design for demonstrating plasmonics in an all-semiconductor platform is shown in Fig. 1(a). The pump wavelength is set to 800 nm, which corresponds to the photon energy above the bandgap of GaAs, and the pump mode is a dielectric slot mode (TE symmetric supermode of the coupled ridge waveguides) that is supported by two closely adjacent ridge waveguides, as shown in Fig. 1(b). Most of the optical power of the pump mode is contained inside the GaAs regions of the waveguide structure, and upon sufficiently high intensity pump excitation, the GaAs regions are rendered metallic while the surrounding GaN remains nonmetallic. The probe is at the telecommunications wavelength of 1550 nm, and the probe mode is a plasmonic gap mode with optical power concentrated in the air region between the two ridge waveguides, due to the GaAs rendered metallic, as shown in Fig. 1(c). A plasmonic gap mode [9] represents the solution of Maxwell's equations for the structure consisting of a nanoscale gap within a thin metal film, which is the two-dimensional analog of the simpler metal–insulator–metal structure [32]. This mode can be considered the coupling of two single interface SPP modes at each of the metal–dielectric boundaries within the structure.

This waveguide structure satisfies the design criteria stated above. First, the fabrication of this device is quite feasible.

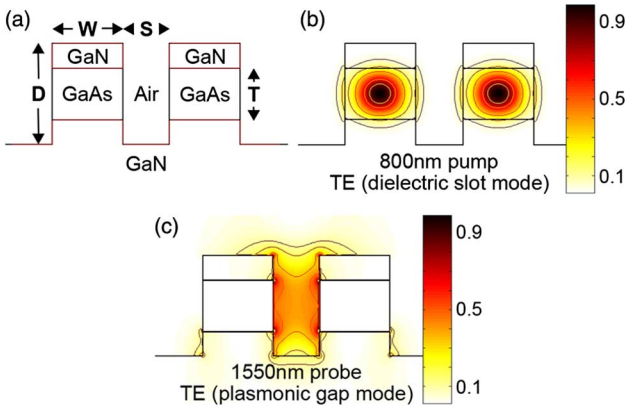

Fig. 1. (Color online) Schematics of the (a) cross section of GaAs/GaN semiconductor plasmonic waveguide with etch depth $D = 400$ nm, ridge width $W = 300$ nm, spacing between ridges $S = 200$ nm, and the GaAs layer thickness $T = 200$ nm, (b) the excitation pump mode electric field intensity profile at $\lambda = 800$ nm, and (c) the probe mode electric field intensity profile at $\lambda = 1550$ nm.

The process would begin with a GaN layer that is several to tens of microns thick. Next, a 200 nm thick layer of GaAs is grown on top, followed by the growth of 100 nm of GaN. The last step would be to pattern the surface and etch to a depth of 400 nm to produce the final waveguide structure. Another criterion that is met would be the ability to clearly distinguish when a plasmonic mode exists, because the waveguide structure does not support any modes at the probe wavelength of 1550 nm in the absence of the pump excitation mode, as a result of the submicron size and two-ridge structure of the waveguide, which only has overall dimensions of 800 nm by 400 nm. This is confirmed by a commercial mode solver. Finally, while the current waveguide structure is already submicron in size, it can be further scaled down, because the size of the plasmonic gap mode is limited only by the cutoff width and height; however, for a symmetric plasmonic gap waveguide, the subwavelength mode is always supported and there is no cutoff [32], which the current waveguide design highly mimics as the GaAs layer is surrounded on both the top and the bottom by GaN of 100 nm thickness. It is not completely symmetric only because of the presence of the GaN substrate. When scaling down the waveguide cross section, the pump excitation mode would cease to exist below certain dimensions due to cutoff, but this problem can be solved by decreasing the wavelength used for the pump.

Another important characteristic of the current plasmonic waveguide design, as shown in Fig. 1(a), is that both the pump and probe modes can be excited directly by a Gaussian beam at the respective wavelengths of 800 and 1550 nm, with reasonably high end-fire coupling efficiencies. The ability to efficiently end-fire couple to both the pump and probe modes of the semiconductor plasmonic waveguide with Gaussian beams simultaneously would help simplify the experimental setup required to characterize the device. First, consider an 800 nm wavelength pump Gaussian beam with a 800 nm waist diameter, which is chosen because it matches well with the cross-sectional size of the waveguide as shown in Fig. 1(a), and it is also quite feasible with a typical objective lens for focusing. At the intensity of 225 GW/cm^2, which corresponds to an average power of 13.2 mW using a 150 fs at 78 MHz repetition rate pulsed laser system, the coupling efficiency to the pump dielectric slot mode as shown in Fig. 1(b) would be approximately 17%. This excitation beam intensity would induce a free carrier concentration of 5.11×10^{21} cm^{-3} in the GaAs regions, leading to $\varepsilon_M \sim -137$ that is sufficient for plasmonic behavior. With the GaAs regions rendered metallic by the pump beam, a probe Gaussian beam at 1550 nm with a waist diameter of 1 μm would have a coupling efficiency to the plasmonic gap mode, as shown in Fig. 1(c), of approximately 21%. It is also useful to consider the average power requirement of a larger diameter excitation beam, because it represents the case when a lower numerical aperture objective lens is used. For demonstration, the same pulsed laser system is utilized but with the pump beam focused to a waist diameter of 3 μm. In this case, the coupling efficiency to the pump dielectric slot mode as shown in Fig. 1(b) is around 5.5%. To achieve the free carrier concentration of 5.11×10^{21} cm^{-3} in the GaAs regions, an excitation beam intensity of 49.3 GW/cm^2 is required, corresponding to an average power of 40.8 mW, which is several times higher than with the pump beam focused to a diameter of 800 nm.

Practically, it must be pointed out that the objective lens used for focusing the excitation beam would cause some pulse broadening due to GVD within the lens material, and this would essentially lower the peak intensity of the pulses. However, this shortcoming can be mitigated by either increasing the average pump intensity or using optics to manage the dispersion that the beam experiences. The detailed calculations of this effect are not included, because the peak intensities achievable by commercial ultrafast laser systems are much higher than what is required for demonstrating the plasmonic effect in semiconductors such as GaAs. Finally, it is noted that the pump-probe experiment described here can be conducted at room temperature.

B. Plasmonic Mode Propagation Characteristics

The properties of the probe plasmonic mode are directly affected by the intensity of the pump excitation, which can be exploited for control of the plasmonic mode and lead to a myriad of functional plasmonic devices. To control the propagation characteristics of the probe plasmonic signal using the pump excitation beam, the pump intensity-dependent properties of the plasmonic mode must be investigated. The optical intensity inside the GaAs regions determines the free carrier density by Eq. (9), and the carrier density sets the dielectric permittivity, as governed by Eqs. (1) and (2). For the pump intensity range used in the study, the low intensity limit corresponds to just above the threshold for the probe plasmonic gap mode to exist in the optically pumped structure, and the high intensity limit corresponds to just below the free carrier concentration of 10^{22} cm^{-3}, which is the threshold for laser-induced material damage for fs laser pulses. The resulting range of average excitation powers is approximately from 15 to 75 mW. The trend in the dielectric permittivity of GaAs as a function of pump intensity of a 3 μm waist diameter Gaussian beam is shown in Fig. 2; the real part of the dielectric permittivity decreases as intensity increases, and the imaginary part increases as the intensity increases.

With information about the dielectric permittivity of the GaAs regions over the range of intensities studied, the different propagation properties of the plasmonic gap mode are obtained using Lumerical MODE Solutions simulation software. The plots in Fig. 3 summarize the different plasmonic mode properties at 1550 nm as a function of the average excitation power of a 3 μm waist diameter Gaussian beam based on a 150 fs pulsed laser at 78 MHz repetition rate, including the effective index (n_{eff}), propagation constant or phase constant (β), modal loss (L), and fraction of plasmonic mode power contained within the air gap region (η). Figure 4 contains the plots of group velocity v_g and group velocity dispersion (GVD) as a function of average pump excitation power.

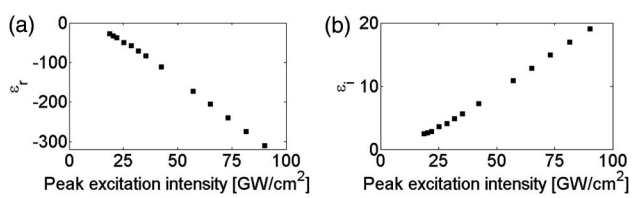

Fig. 2. Plots of (a) real part (ε_r) and (b) imaginary part (ε_i) of the dielectric permittivity of GaAs as a function of the pump excitation peak intensity.

As the pump intensity is increased, the free carrier concentration in the GaAs metallic layer increases, resulting in less EM field penetration inside the metal. This effect essentially causes all the trends seen in Figs. 3 and 4. As the field penetration inside the metallic GaAs decreases, a higher fraction (η) of the plasmonic mode power resides in the air gap region, which means the effective index (n_{eff}) would decrease to become closer to that of air, and the phase constant (β) would also decrease. As the EM field is pushed away from the highly lossy metallic GaAs, the propagation loss (L) would decrease; and conversely, the plasmonic mode would propagate over a larger distance. The reduction in plasmonic mode propagation loss as the semiconductor becomes more "metallic" due to the increase in carrier concentration does not contradict the motivation for using semiconductors over metals for plasmonics at the outset of this paper. This highlights another benefit of using optical excitation to transform a semiconductor to a metal, which is the flexibility of how metallic the semiconductor material can become. This point is more subtle in its effects, because inducing a carrier concentration just above the threshold to support a plasmonic mode can provide lower ohmic loss compared to the case if a natural metal is used. However, increasing the carrier concentration beyond what is needed to support a plasmonic mode increases the ohmic loss of EM fields within the metallic semiconductor, but at the same time the overall loss of the propagating plasmonic mode would decrease.

The last two plasmonic mode propagation parameters are the group velocity (v_g), which increases as the pump intensity is increased, just like the trend for phase velocity, and the GVD that can be tuned from positive to negative values

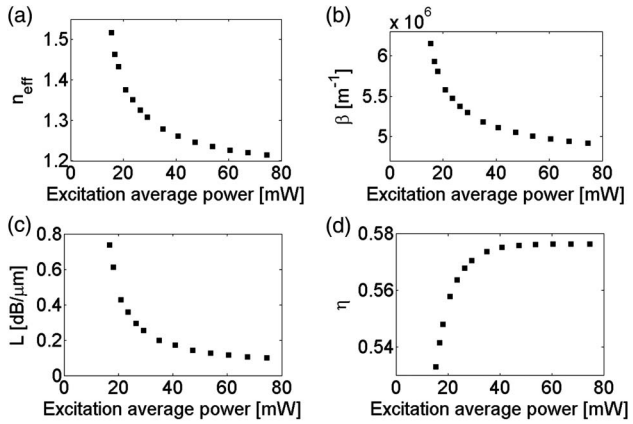

Fig. 3. Plots of 1550 nm wavelength probe plasmonic gap mode properties as a function of average excitation power, including the (a) effective index (n_{eff}), (b) phase constant (β), (c) modal loss (L), and (d) fraction of mode power in the air gap region (η).

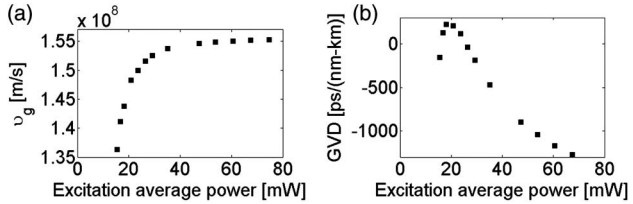

Fig. 4. Plots of (a) group velocity (v_g) and (b) GVD of 1550 nm wavelength probe plasmonic gap mode as a function of average excitation power.

depending on the pump intensity. This has important implications for high speed transmission systems, as group velocity is essentially the speed of optical pulse propagation and GVD is a measure of the broadening of pulses during propagation.

It is constructive to compare this work with previous work, where the control of optical properties in plasmonic structures has been largely limited to the nonmetallic dielectric layers. Techniques that are similar to what is presented in this paper have been studied, such as in [33], where ultrafast fs optical pulses incident on an aluminum metal surface are used to disturb the equilibrium in the energy-momentum distribution of electrons and influence SPP propagation along the surface. Also, in [34], ultrafast fs pulses are used to generate free carriers in ion-implanted silicon that leads to changes in the dielectric properties. However, the technique is based on increasing the imaginary part of the dielectric permittivity ε_i, which increases the absorption as a result of photogenerated free carriers. To our knowledge, the present paper is the first theoretical work to investigate the modification of the real part of the dielectric permittivity ε_r of a semiconductor material within an all-semiconductor structure for the manipulation of optical frequencies SPP propagation.

5. CONCLUSIONS

We investigated the feasibility of sustaining plasmonic modes in an all-semiconductor platform based on ultrahigh optical intensity free carrier generation that causes certain regions to effectively transform into a metal. After a review of the current status of semiconductor plasmonics, such as operation in the THz frequencies and using doping or electrical injection as techniques for increasing free carrier concentration, the route of optical excitation with mainstay semiconductors such as GaAs is discovered to be quite attainable with the use of readily available ultrafast laser systems. A detailed calculation of the required intensities to induce the necessary changes in optical properties of the semiconductor is then carried out, which took into account critical nonlinear optical effects. Next, a semiconductor plasmonic waveguide design based on the GaAs/GaN materials system is presented, which satisfies several key design criteria, such as being amenable for fabrication with currently available technologies, the testability with a relatively simple optical characterization setup, and also the subdiffraction-limited cross section that can be further scaled down. Last, the novel concept of changes in the plasmonic mode propagation characteristics as a function of excitation pump intensity is investigated and explained in detail. In conclusion, we have theoretically shown that all-semiconductor plasmonics at optical frequencies is indeed quite feasible, and furthermore, that the ideas investigated can be useful for functional plasmonic devices, which are well worth studying further.

ACKNOWLEDGMENTS

The authors would like to acknowledge NSERC for their financial support.

REFERENCES

1. S. Maier, *Plasmonics—Fundamentals and Applications* (Springer, 2007).
2. M. Kuttge, E. J. R. Vesseur, J. Verhoeven, H. J. Lezec, and H. A. Atwater, "Loss mechanisms of surface plasmon polaritons on gold probed by cathodoluminescence imaging spectroscopy," Appl. Phys. Lett. **93**, 113110 (2008).
3. T. Sands, J. P. Harbison, N. Tabatabaie, W. K. Chan, H. L. Gilchrist, T. L. Cheeks, L. T. Florez, and V. G. Keramidas, "Epitaxial metal(NiAl)-semiconductor(III-V) heterostructures by MBE," Surf. Sci. **228**, 1–8 (1990).
4. M. G. Blaber, M. D. Arnold, and M. J. Ford, "A review of the optical properties of alloys and intermetallics for plasmonics," J. Phys. Condens. Matter **22**, 143201 (2010).
5. V. A. Fedotov, T. Uchino, and J. Y. Ou, "Low-loss plasmonic metal material based on epitaxial gold monocrystal film," Opt. Express **20**, 9545–9550 (2012).
6. J. Grandidier, G. Colas des Francs, S. Massenot, A. Bouhelier, L. Markey, J.-C. Weeber, C. Finot, and J. Dereux, "Gain-assisted propagation in a plasmonic waveguide at telecom wavelength," Nano Lett. **9**, 2935–2939 (2009).
7. M. Z. Alam, J. Meier, J. S. Aitchison, and M. Mojahedi, "Propagation characteristics of hybrid modes supported by metal-low-high index waveguides and bends," Opt. Express **18**, 12971–12979 (2010).
8. L. Pavesi and D. J. Lockwood, *Silicon Photonics* (Springer, 2004).
9. D. F. Pile, T. Ogawa, D. K. Gramotnev, Y. Matsuzaki, and K. C. Vernon, "Two-dimensionally localized modes of a nanoscale gap plasmon waveguide," Appl. Phys. Lett. **87**, 261114 (2005).
10. T. H. Isaac, W. L. Barnes, and E. Hendry, "Determining the terahertz optical properties of subwavelength films using semiconductor surface plasmons," Appl. Phys. Lett. **93**, 241115 (2008).
11. J. Gómez Rivas, M. Kuttge, P. Haring Bolivar, and H. Kurz, "Propagation of surface plasmon polaritons on semiconductor gratings," Phys. Rev. Lett. **93**, 256804 (2004).
12. E. Hendry, F. J. Garcia-Vidal, L. Martin-Moreno, J. Gómez Rivas, M. Bonn, A. P. Hibbins, and M. J. Lockyear, "Optical control over surface-plasmon-polariton-assisted THz transmission through a slit aperture," Phys. Rev. Lett. **100**, 123901 (2008).
13. G. V. Naik, J. Liu, A. V. Kildishev, V. M. Shalaev, and A. Boltasseva, "Demonstrations of Al:ZnO as a plasmonic component for near-infrared metamaterials," Proc. Natl. Acad. Sci. USA **109**, 8834–8838 (2011).
14. G. V. Naik, J. L. Schroeder, X. Ni, A. V. Kildishev, T. D. Sands, and A. Boltasseva, "Titanium nitride as a plasmonic material for visible and near-infrared wavelengths," Opt. Mater. Express **2**, 478–489 (2012).
15. G. V. Naik and A. Boltasseva, "Semiconductors for plasmonics and metamaterials," Phys. Status Solidi Rapid Res. Lett. **4**, 295–297 (2011).
16. D. Li and C. Z. Ning, "All-semiconductor active plasmonic system in mid-infrared wavelengths," Opt. Express **19**, 14594–14603 (2011).
17. M. Durach, A. Rusina, M. F. Kling, and M. I. Stockman, "Metallization of nanofilms in strong adiabatic electric fields," Phys. Rev. Lett. **105**, 086803 (2010).
18. A. Schiffrin, T. Paasch-Colberg, N. Karpowicz, V. Apalkov, D. Gerster, S. Mühlbrandt, M. Korbman, J. Reichert, M. Schultze, S. Holzner, J. V. Barth, R. Kienberger, R. Ernstorfer, V. S. Yakovlev, M. I. Stockman, and F. Krausz, "Optical-field-induced current in dielectrics," Nature **493**, 70–74 (2012).
19. M. Schultze, E. M. Bothschafter, A. Sommer, S. Holzner, W. Schweinberger, M. Fiess, M. Hofstetter, R. Kienberger, V. Apalkov, V. S. Yakovlev, M. I. Stockman, and F. Krausz, "Controlling dielectrics with the electric field of light," Nature **493**, 75–78 (2012).
20. D. M. Goodmanson, "A recursion relation for matrix elements of the quantum bouncer," Am. J. Phys. **68**, 866–868 (2000).
21. C. Zener, "Non-adiabatic crossing of energy levels," Proc. R. Soc. A **137**, 696–702 (1932).
22. A. N. Oraevsky, "Whether is it possible to produce high concentrations of carriers in a semiconductor for observing the Bose condensate at room temperature?" Quantum Electron. **33**, 377–379 (2003).
23. M. Rasolt, "Plasmon-phonon-assisted electron-hole recombination in Si at very high carrier density," Phys. Rev. B **33**, 1166–1176 (1986).

24. H. M. van Driel, "Kinetics of high-density plasmas generated in Si by 1.06- and 0.53 μm picosecond laser pulses," Phys. Rev. B **35**, 8166–8176 (1987).
25. M. Combescot and J. Bok, "Electron-hole plasma generation and evolution in semiconductors," J. Lumin. **30**, 1–17 (1985).
26. R. Schroeder and B. Ullrich, "Absorption and subsequent emission saturation of two-photon excited materials: theory and experiment," Opt. Lett. **27**, 1285–1287 (2002).
27. J. K. Chen, D. Y. Tzou, and J. E. Beraun, "Numerical investigation of ultrashort laser damage in semiconductors," Int. J. Heat Mass Transfer **48**, 501–509 (2005).
28. P. Allenspacher, B. Hüttner, and W. Riede, "Ultrashort pulse damage of Si and Ge semiconductors," Proc. SPIE **4932**, 359–365 (2003).
29. K. Sokolowski-Tinten and D. von der Linde, "Generation of dense electron-hole plasmas in silicon," Phys. Rev. B **61**, 2643–2650 (2000).
30. P. Saeta, J.-K. Wang, Y. Siegal, N. Bloembergen, and E. Mazur, "Ultrafast electronic disordering during femtosecond laser melting of GaAs," Phys. Rev. Lett. **67**, 1023–1026 (1991).
31. S. V. Novikov, N. M. Stanton, R. P. Campion, R. D. Morris, H. L. Geen, C. T. Foxon, and A. J. Kent, "Growth and characterization of free-standing zinc-blende (cubic) GaN layers and substrates," Semicond. Sci. Technol. **23**, 015018 (2008).
32. G. Veronis and S. Fan, "Modes of subwavelength plasmonic slot waveguides," J. Lightwave Technol. **25**, 2511–2521 (2007).
33. K. F. MacDonald, Z. L. Sámson, M. I. Stockman, and N. I. Zheludev, "Ultrafast active plasmonics," Nat. Photonics **3**, 55–58 (2008).
34. A. Y. Elezzabi, Z. Han, S. Sederberg, and V. Van, "Ultrafast all-optical modulation in silicon-based nanoplasmonic devices," Opt. Express **17**, 11045–11056 (2009).